Theoretical and Experimental Investigation of the UV Cross Section and Kinetics of the Methyl Formate Peroxy Radical

Jaron C. Hansen, Yumin Li, Claudette M. Rosado-Reyes, and Joseph S. Francisco*

Department of Chemistry and Department of Earth and Atmospheric Sciences, Purdue University, West Lafayette, Indiana 47907

Joseph J. Szente and M. Matti Maricq*

Research laboratory, Ford Motor Company, P.O. Box 2053, Drop 3083, Dearborn, Michigan 48121

Received: May 9, 2002; In Final Form: March 12, 2003

Flash photolysis combined with UV time-resolved spectroscopy has been utilized to investigate the composite UV cross section for methyl formate peroxy ($CH_3OC(O)O_2$ and $O_2CH_2OC(O)H$) between 210 and 320 nm. The self-reaction rate constant for methyl formate peroxy was measured at 298 K and found to be $(2.3 \pm 0.7) \times 10^{-11}$ cm^3 molecule^{-1} s^{-1}. Evidence is reported for the production of OH radical and CH_2O from the decomposition of the activated methyl formate peroxy radical produced by the addition of O_2 to methyl formate radical, and for the formation of ClO from the Cl + peroxy reaction. High level ab initio calculations were performed to explore the methyl formate oxidation mechanism as well as to assign the experimentally observed UV spectrum. The calculated UV spectrum band center is found to be within 10% of the experimentally determined methyl formate peroxy spectrum. High-resolution IR detection of the CH_2O fragment was used to probe the branching ratio for unimolecular dissociation relative to collisional stabilization of the activated methyl formate peroxy radical as a function of pressure. The dissociation kinetics is described using a modified Lindemann mechanism.

I. Introduction

Organic peroxy radicals represent an important class of molecules with atmospheric implications. They are produced in the atmosphere by the hydroxyl radical initiated oxidation of hydrocarbon molecules, followed by the addition of O_2 to the hydrocarbon radical. Laboratory studies often substitute chlorine atoms to initiate the oxidation chemistry. In urban environments RO_2 radicals can react with NO and as a consequence promote O_3 formation.[1] In a clean atmosphere (i.e., low NO_x environment), the principle fate of RO_2 radicals is reaction with other peroxy radicals, such as HO_2.[1] Oxygenated hydrocarbons such as dimethyl ether and dimethoxymethane have been proposed as substitutes or additives to diesel fuel.[2−5] Although dimethyl ether has been shown to have a favorable impact on diesel engine combustion, the fate of the combustion products is just beginning to be reported.[6−9] Methyl formate ($CH_3OC(O)H$) has been found to be a product of the oxidation of dimethyl ether in the atmosphere.[10] It is expected that the atmospheric degradation of methyl formate will proceed via the methyl formate peroxy radicals ($CH_3OC(O)O_2$ and $O_2CH_2OC(O)H$), which can then undergo reaction with other peroxy radicals or with NO_x.

High level ab initio calculations are presented to help interpret the experimental measurements of the UV spectrum, degradation pathways, and subsequent products from the chlorine and fluorine atom initiated oxidation of methyl formate. The calculated vertical excitation energies for the methyl formate peroxy radical help support the deconvolution of the experimental spectra that arise from the two peroxy isomers produced from the hydrogen atom abstraction by halogen atoms. The ab initio calculations lend insight into the reaction pathways responsible for rearrangement and subsequent dissociation of the nascent peroxy radicals formed by the addition of O_2 to the two isomeric methyl formate radicals. The benefits of combining experimental and ab initio methods to the study of methyl formate oxidation and spectroscopy can be extrapolated to other peroxy radicals.

II. Methods

A. Experimental Methods. Flash photolysis/UV time-resolved spectroscopy is used to measure the UV spectrum of methyl formate peroxy radical as well as a probe for evidence of OH and ClO radicals. A high resolution continuous-wave (cw) Pb-salt IR diode laser (9 MHz fwhm) is used to detect CH_2O. The details of this apparatus have been described previously.[11,12] As such, only a summary is given here. The reagent gases are introduced into a 52.8 cm long by 3.5 cm diameter cylindrical flow cell operating under slow flow conditions. The gas flows are adjusted with Tylan/Millipore mass flow controllers to produce a variety of reagent gas compositions from which methyl formate peroxy radicals are formed. For these experiments, the gas mixtures consisted of methyl formate (∼2−6 Torr), 4.8% chlorine/N_2 (∼2−5 Torr) or 10% fluorine/N_2 (∼20−40 Torr), O_2 (∼20−50 Torr), and N_2 to make up the balance. Using these partial pressures the total pressure in the reaction cell ranges between 10 and 230 Torr. Under these conditions there is a complete renewal of reagent gases in the flow cell every 1.5−3 s. The hydrogen extraction from methyl formate by atomic chlorine (or fluorine) is initiated by firing a Lambda Physik model LPX 301 excimer laser into the gas mixture at a repetition rate of 1.5 s per pulse, lasing at 351 nm, and having an output energy of either 300 or

10.1021/jp021180x CCC: $25.00
Published on Web 06/18/2003

600 mJ per pulse. This generates $(2-12) \times 10^{14}$ molecules cm^{-3} of Cl atoms (F atoms) per pulse.

The time-resolved UV spectroscopy is performed as follows. The output from a 75 W deuterium lamp passes through the flow cell and then enters a monochromator (Instruments SA, HR320) with a 147 line/mm grating that separates the spectral features onto a linear diode array (Princeton Instruments IPDA-700). The resulting spectra have a fwhm resolution of 2−3 nm. A background UV spectrum over the range of 200−340 nm is obtained before the reaction is initiated. At preset delay times after the laser fires, a second spectrum is collected. The absorbance spectrum is then calculated using Beer's law (absorbance $= -\ln(I/I_0)$), where I_0 is the intensity of the light before the laser is fired and I is the intensity of the light at the selected delay time after the laser fires. In general, 500 spectra are co-added and averaged to generate an absorption spectrum for methyl formate peroxy. When probing for OH and ClO radicals, the detector array is mounted to a higher resolution monochromator with a 600 line/mm grating set to cover the wavelength range between 275 and 320 nm. These spectra have a fwhm resolution of 0.3 nm, which makes it possible to distinguish the characteristic spectral features of both OH and ClO radicals. Due to the greater dispersion of light by the high-resolution monochromator, less light impinges on each diode; therefore 2500 spectra are averaged to generate an absorption spectrum with suitable S/N. Wavelength calibration is verified with spectral lines from a low-pressure Hg lamp.

The transient IR absorption measurements are performed as follows. A high-resolution diode laser is used to probe a $v = 0$ to $v = 1$ rovibrational carbonyl stretch transition of CH_2O at a frequency of 1709 cm^{-1}. The output from a cryogenically cooled Pb-salt diode is passed through a mode selecting monochromator and is then directed through the reaction cell. After passing through the cell, the IR light is directed through a second monochromator to prevent extraneous light from the excimer laser from reaching the detector. The IR light is then focused on a LN_2 cooled HgCdTe detector with a response time of 0.3 μs. Measurements are made over both a 50 μs and a 1 ms time scale after photolysis.

The initial halogen radical concentration is determined by substituting ethane for methyl formate into the reaction mixture for each set of conditions and measuring the corresponding ethyl peroxy UV absorbance spectrum over the wavelength range 200−300 nm. The cross section for ethyl peroxy radical is well studied[13] and provides a suitable reference for determining the initial halogen radical concentration from the ethyl peroxy yield. A small correction is included to account for minor interfering reactions that reduce the yield from 100% to ∼95%.

The measured UV absorption spectra taken of the methyl formate/chlorine or fluorine/oxygen/nitrogen reaction mixtures have contributions from several UV absorbing compounds over the 200−325 nm range. Deconvolving the transient spectra into their individual absorbing components and number densities was necessary to determine the UV absorption spectrum of the methyl formate peroxy radical as well as the kinetics of its self-reaction. The overall absorbance spectrum that is measured can be described by the following linear combination:

$$A_{\text{total}} = \sum [C_i]\sigma_{C_i} l \qquad (1)$$

where A_{total} is the total measured absorbance at a given delay time, $[C_i]$ is the change in concentration of the absorbing compound, σ_{C_i} is the cross section for the corresponding compound, and l is the path length. For these experiments, compounds of interest include the methyl formate peroxy radical, Cl_2, methyl formate, OH, and ClO. Measurements used to determine the methyl formate peroxy radical cross sections were made at early delay times, 10−20 μs, following Cl_2 (or F_2) photolysis, and at total pressures above 150 Torr. These conditions were selected to minimize the effects of reactions that remove the peroxy radicals, including unimolecular dissociation of the radical. Measurements of the OH radical were performed at early delay times when the OH concentration is expected to be at a maximum, and at total pressures of 20, 50, and 220 Torr to confirm the dependence of OH yield on total pressure. To measure the methyl formate peroxy self-reaction rate constant, UV spectra were collected at a variety of discrete delay times between 10 μs and 1.0 ms at total pressures between 20 and 220 Torr.

Transient IR measurements of the formation of CH_2O during the first 20 μs after the photolysis laser pulse were used to predict the fraction of the nascent methyl formate peroxy radicals that dissociate (see reactions 7 and 8 in Table 5). IR traces were recorded using chlorine atom initiation at pressures between 10 and 220 Torr. Fluorine was not used because a relatively high concentration is required to generate a sufficient amount of fluorine atoms (using 351 nm photolysis) and limits the reduction in total pressure. To quantify the CH_2O concentration, it was necessary to determine the IR cross section for CH_2O at the 1709 cm^{-1} absorbance line for the pressures used in this study. This was accomplished by substituting CH_3OH for methyl formate in the reaction gas mixture. Methanol oxidation proceeds as follows:

$$CH_3OH + Cl \rightarrow CH_2OH + HCl$$

$$CH_2OH + O_2 \rightarrow CH_2O + HO_2$$

Under the conditions used in this study, these two reactions proceed quickly, <5 μs, generating CH_2O and HO_2 radicals. Because there is essentially no loss of CH_2O following the second reaction, on the 50 μs time scale, its yield is used to calculate the absorbance cross section of CH_2O at the pressures of the methyl formate experiments.

B. Computational Methods. Ab initio molecular orbital calculations were performed using the GAUSSIAN 98 suite of programs.[14] Geometry optimizations were performed using Hartree−Fock (HF) and second-order Møller−Plesset perturbation theory (MP2) using the 6-31G(d) basis set, on all species involved in the formation and subsequent unimolecular dissociation of the $CH_3OC(O)O_2$ species. These include, $CH_3OC(O)$, $CH_3OC(O)O_2$, $CH_2OC(O)O_2H$, $HC(O)H$, CO_2, and OH radical. In addition, the transition states involved in the decomposition of $CH_3OC(O)O_2$ were identified. All optimizations were carried out to better than 0.001 Å for bond lengths and 0.1° for angles, with a self-consistent field convergence of at least 10^{-7} for reactants, products, and transition states on the density matrix. The residual rms force was less than 10^{-4} atomic units. These parameters were used to verify that the minimum energy structure had been identified for each species. The vibrational frequencies and estimates of the zero point energies were performed for each species involved in the $CH_3OC(O)O_2$ potential energy surface using the optimized geometry found at the MP2/6-31G(d) level. One imaginary frequency was found for each transition state, verifying their location as a maximum in one coordinate of the potential energy surface. To refine the energies and geometries, optimizations were performed using the Gaussian-2, second-order variant (G2(MP2)) and complete basis set (CBSQ) composite methods. Heats of reaction and

TABLE 1: Total Energies (hartrees) for Methyl Formate Radical, Methyl Formate Peroxy, the Unimolecular Decomposition Products, and the Transition States at 298 K

species	MP2/6-31G(d)	G2MP2	CBSQ
$CH_3OC(O)$	−227.75883	−228.06403	−228.08015
$CH_3OC(O)OO$	−377.75688	−378.26748	−378.29954
$CH_2OC(O)OOH$	−377.74625	−378.25922	−378.29180
HC(O)H	−114.17495	−114.33606	−114.34272
CO_2	−188.11836	−188.35661	−188.37122
OH	−75.52320	−75.64092	−75.64887
O_2	−149.95431	−150.14207	−150.16274

transition states	MP2/6-31G(d)	G2MP2	CBSQ
$[CH_3OC(O)OO \rightarrow CH_2OC(O)OOH]^{\ddagger -}$	−377.70099	−378.25262	−378.28346
$[CH_2OC(O)OOH \rightarrow HC(O)H + CO_2 + OH]^{\ddagger}$	−377.71072	−378.24393	−378.27671

TABLE 2: Heat of Reactions and Activation Energies Calculated Using a Number of ab Initio and Composite Methods (kcal mol^{-1})

	heat of reaction[a,b]			activation energies[a,b]		
reaction	MP2/6-31G(d)	G2MP2	CBSQ	MP2/6-31G(d)	G2MP2	CBSQ
$CH_3OC(O) + O_2 \rightarrow CH_3OC(O)O_2$	−24.0	−35.0	−32.1			
$CH_3OC(O)O_2 \rightarrow CH_2OC(O)OOH$	5.1	3.6	3.3	31.7	6.0	6.7
$CH_2OC(O)OOH \rightarrow HC(O)H + CO_2 + OH$	−50.1	−52.7	−50.6	19.9	7.2	7.1

[a] Units are given in kcal mol^{-1}. [b] Energies include zero point energy correction.

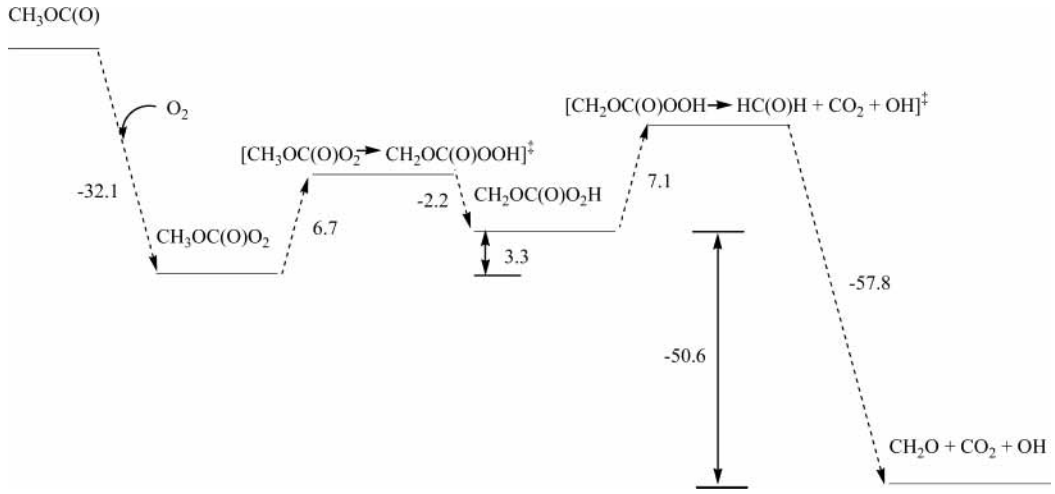

Figure 1. Potential energy surface for the formation of methyl formate peroxy and its subsequent unimolecular dissociation.

activation energies were calculated to characterize the energetics of the potential energy surface of the reaction mechanism. Enthalpies of reaction ($\Delta_{rxn}H_{298}$) were obtained by calculation of the absolute energy for each species involved in the reaction. The difference in the sum of the absolute energies of the reactants and products with zero point energy correction was used to calculate the enthalpy of reaction ($\Delta_{rxn}H_{298}$).

The excited states were calculated with complete active space self-consistent field (CASSCF) method.[15,16] The CASSCF calculations were performed using the MOLPRO96 program.[17] The active space used for the CASSCF was (9 electron, 9 orbital).

III. Results

A. Computations. *1. Thermodynamics of the Methyl Formate Radical + O_2 Reaction.* The absolute energies calculated using a number of ab initio and composite methods are listed in Table 1. Different methods were used to verify convergence to a uniform value. The relative energies are listed in Table 2. The values at the MP2/6-31G(d), G2MP2 and CBSQ incorporate the zero point energy correction at the MP2/6-31G(d) level of theory. Figure 1 illustrates the potential energy surface for the $CH_3OC(O)$ radical, the major product from hydrogen abstraction by chlorine atoms. The thermodynamics and corresponding potential energy surface are expected to be similar for the $CH_2OC(O)H$ radical. The addition of O_2 to the methyl formate radical is thermodynamically favored, being exothermic by −32.1 kcal mol^{-1}. Which is in good agreement with previous calculations by Good et al., which reports a value of 36.4 kcal mol^{-1}.[7] The rearrangement of methyl formate peroxy radical into the acyloxymethyl radical proceeds over an energy barrier of 6.7 kcal mol^{-1} relative to methyl formate peroxy. Due to the large exothermicity of the initial peroxy formation, it is not unreasonable to expect some fraction of methyl formate peroxy to proceed through this channel. Once over the barrier, formation of the $CH_2OC(O)O_2H$ radical is calculated to be exothermic by −2.2 kcal mol^{-1} relative to the transition state. The unimolecular decomposition of $CH_2OC(O)O_2H$ is predicted to be thermodynamically and kinetically favored, proceeding with an activation energy of 7.1 kcal mol^{-1}, and having a large reaction enthalpy of −50.6 kcal mol^{-1} relative to $CH_2OC(O)O_2H$.

2. Thermodynamics of the Methyl Formate + F Reaction. Calculations were performed in a previous study[8] using the second-order Møller−Plesset method and the G2 and G2MP2

TABLE 3: Absolute Energies (hartrees) for the F + $CH_3OC(O)H$ Reaction

level of theory	F	HF	$CH_3OC(O)H$	$CH_2OC(O)H$	$CH_3OC(O)$	methyl H extraction transition state	formyl H extraction transition state
QCISD/6-31G(d)	−99.49795	−100.18691	−228.42217	−227.76460	−227.769003	−327.91280	−327.91569
QCISD/6-311G(d,p)	−99.56415	−100.27050	−228.55303	−227.88733	−227.891591	−328.11171	−328.11360
QCISD(T)/6-311++G(d,p)	−99.57168	−100.28530	−228.58828	−227.9217	−227.925972	−328.15875	−328.15941
QCISD(T)/6-311++G(2d,2p)	−99.59208	−100.30986	−228.64242	−227.97451	−227.977933	−328.23498	−328.23577
QCISD(T)/6-311++G(2df,2p)	−99.61391	−100.33312	−228.71347	−228.04495	−228.047631	−328.3281	−328.32867
ZPE QCISD/6-31G(d) (kcal mol^{-1})	0	5.7	39.7	30.4	31.8	37.1	38.1

TABLE 4: Heats of Reaction and Activation Barriers for the F + $CH_3OC(O)H$ Reaction (kcal mol^{-1})

level of theory	H_{rxn}[$CH_3OC(O)H + F \rightarrow CH_2OC(O)H + HF$]	H_{rxn}[$CH_3OC(O)H + F \rightarrow CH_3OC(O) + HF$]	E_a (methyl H extraction)	E_a (formyl H extraction)
QCISD/6-31G(d)	−23.3	−24.6	2.0	1.2
QCISD/6-311G(d,p)	−29.1	−30.3	0.8	0.7
QCISD(T)/6-311++G(d,p)	−33.1	−34.3	−1.8	−1.2
QCISD(T)/6-311++G(2d,2p)	−34.9	−35.6	−2.9	−2.4
QCISD(T)/6-311++G(2df,2p)	−35.4	−35.6	−3.1	−2.4

methodologies on the Cl + $CH_3OC(O)H$ reaction to determine the branching ratio of hydrogen abstraction from methyl formate. Because the present study includes F + methyl formate chemistry, it was important to probe the potential energy surface of this reaction. Fluorine atoms are more reactive than chlorine atoms; consequently, it is expected that fluorine atoms will be less discriminate than chlorine atoms for the hydrogen that it will extract from methyl formate. As such, a different ratio of $CH_3OC(O)$ and $CH_2OC(O)H$ radicals, and subsequent $CH_3OC(O)O_2$ and $O_2CH_2OC(O)H$ radicals will be produced as a result of the use of fluorine versus chlorine as the radical precursor. The absolute energies for all of the species involved in the F + $CH_3OC(O)H$ reaction including F, $CH_3OC(O)H$, $CH_2OC(O)H$, $CH_3OC(O)$, and HF are given in Table 3. The activation barriers and heats of reaction for both methyl formate radicals ($CH_3OC(O)$ and $CH_2OC(O)H$) are reported in Table 4. All values have been corrected for zero point energy. Evaluation of the activation barrier for both pathways shows that at the QCISD/6-31G(d) level a modest barrier of 2.0 kcal mol^{-1} for extraction of a methyl hydrogen and 1.2 kcal mol^{-1} for extraction of the carbonyl hydrogen. As the basis set is increased, the energy barrier for both paths decreases. At the highest level, QCISD(T)/6-311++G(2df,2p) the activation barrier for both pathways is calculated to be lower in energy than the reactants. This effectively means the activation barrier is nonexistent for either path and that the reactivity of the two unequivalent hydrogens will be a function of the preexponential *A* factor in the Arrhenius expression. Transition state theory was used to calculate the preexponential *A* factor for extraction of either hydrogen. The functional form used is

$$k = L\frac{k_b T}{h}\left(\frac{Q_{trans}}{Q_F Q_{CH_3OCOH}}\right)e^{-E/RT} \qquad (2)$$

where k_b is the Boltzmann constant, *L* is the degeneracy factor, *T* is the temperature in Kelvin, and *h* is Planck's constant. Q_{trans} is the product of the individual partition coefficients for the transition state. Q_F and Q_{CH_3OCOH} represent the product of the individual partition coefficients for fluorine atoms and methyl formate, respectively. *E* is the calculated activation barrier and *R* is the gas constant. The ratio of the calculated preexponential *A* factors is the branching ratio for extraction of a methyl hydrogen relative to the carbonyl hydrogen by fluorine atom. This analysis calculates an 81% probability for extraction of a methyl hydrogen and thus 19% probability of extraction of the carbonyl hydrogen. The largest source of uncertainty in the calculation of the branching ratio is due to the treatment of the vibrational modes as harmonic oscillators, especially the low-frequency modes that are populated at room temperature. The effect on the deconvolved methyl formate peroxy cross sections as a result of a ±10% uncertainty in the F + methyl formate branching ratio is described in detail in section B-3 of the Results.

3. Geometry and Vibrational Frequencies of Methyl Formate Peroxy. The optimized geometry for all the species and the transition states involved in the oxidation of methyl formate radical are listed in Supplemental Table 1 which is included as Supporting Information. The corresponding optimized structures are illustrated in Figure 2a−e. The addition of O_2 to methyl formate radical (Figure 2a), producing methyl formate peroxy (Figure 2b) barely modifies the structure of the methyl formate radical. The CO′ bond length is unaffected by the addition of O_2 to the methyl formate radical and the C′O′ bond length decreases by a trivial 0.009 Å. After the addition of O_2 the molecule adopts a *trans* planar configuration with respect to the carbonyl group CO, making the dihedral angle OCO″O‴ equal to 180.0°. The dihedral angles of OCO′C′ and CO′C′H remain the same, with values of 0.0° and 180.0°, respectively. Compared to methyl formate radical, the OCO′ and C′O′C angles in methyl formate peroxy decrease by 0.1° and 0.8°, respectively.

The first transition state involved in the unimolecular degradation of methyl formate peroxy involves the shift of a methyl hydrogen to the terminal oxygen in the peroxy moiety. The transition state minimum-energy structure is given in Figure 2c. The O′CO″ angle increases from 103.8° to 114.4°, and the breaking CH bond elongates by 14% from 1.086 to 1.260 Å. The O″O‴ bond stretches from 1.332 to 1.458 Å to accommodate the hydrogen atom attaching to the O_2 group. The forming O‴H bond shortens from 1.237 Å in the transition state to 0.989 Å in the acyloxymethyl radical $CH_2OC(O)O_2H$ (Figure 2d).

$CH_2OC(O)O_2H$ closely resembles a planar molecule. The two equivalent hydrogen atoms align themselves in plane with the carbonyl group. In addition, the hydrogen atom on the peroxy group is in the plane with the hydrogen atoms on the methyl carbon. The CO′C′H′ and CO″O‴H dihedral angles have values of 18.7° and 1.4°, respectively.

Figure 2e illustrates the transition state in which the acyloxymethyl radical decomposes to form CH_2O, CO_2, and OH radicals. At the transition state the CO′ bond is almost

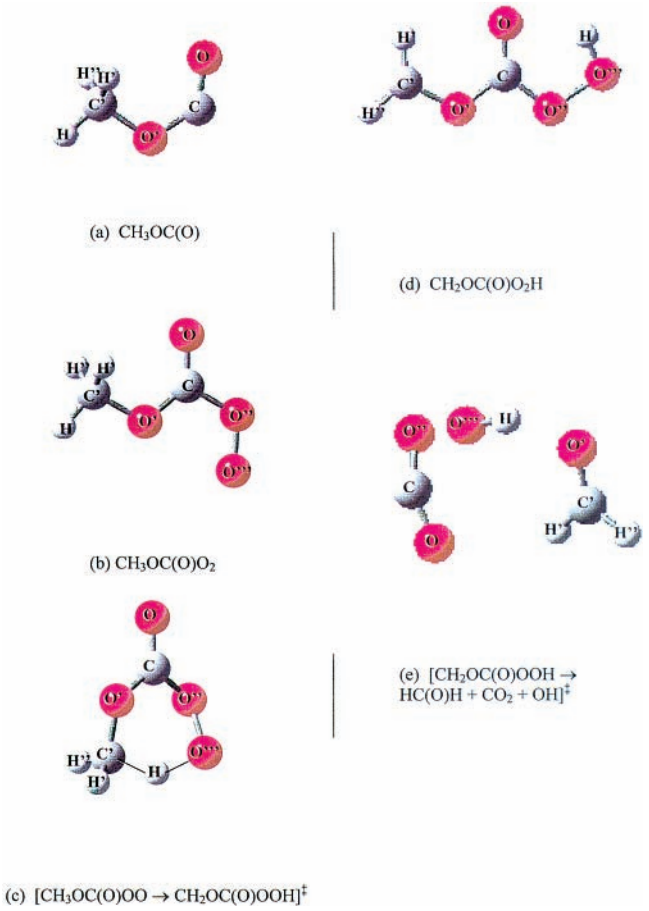

Figure 2. Optimized structures for the species involved in the formation and unimolecular dissociation of methyl formate peroxy.

completely broken, with a value of 3.042 Å. The decomposition products are clearly identified in the transition state structure.

Supplemental Table 2 lists the vibrational frequencies for methyl formate, methyl formate peroxy, and the decomposition products, CH_2O, CO_2, and OH radical and is included as Supporting Information. The vibrational frequencies for the transition states are listed in Supplemental Table 3. Both transition states have large imaginary frequencies, suggesting a narrow passage through the energy barrier.

B. Experimental Measurements. Three aspects of the methyl formate peroxy radical were measured in this experiment: the pressure dependent stabilization versus dissociation of the activated peroxy radical, the UV spectrum, and the peroxy self-reaction rate constant at 298 K. Prior to calculating either the absorption spectra or self-reaction rate constant, it was necessary to quantify the fraction of peroxy radicals lost to interfering reactions. This required the additional consideration of (1) the branching ratio for hydrogen abstraction from methyl formate and (2) the impact of the reaction between the peroxy radicals and Cl atoms.

The oxidation of methyl formate is expected to proceed via the mechanism shown in Table 5 and will be briefly reviewed before presenting the results. Known rate constants are listed along with appropriate references. Estimated rate constants are based on analogous reactions at 298 K, usually substituting either the ethyl radical or acetyl radical for the methyl formate radical and using an average value for those reactions from the NIST chemical kinetics database.[18] All of the rate constants, except for k_6, are either pressure independent or are assumed to be at their high-pressure limit. Where appropriate, R is used in the table to represent either one of the two methyl formate radical isomers (CH_3OCO or $CH_2OC(O)H$). However, in the kinetics model each isomer is assigned a separate reaction equation because the products of these reactions will be different. The initial reactions are typical of alkyl peroxy radical formation; hydrogen abstraction from methyl formate by reaction with Cl (or F) atoms produces the methyl formate radical, which then quickly adds O_2 to produce the corresponding peroxy radical (reactions 1 and 2). Conditions were carefully chosen to reduce the loss of methyl formate radical via competing reactions with halogen atoms or via self-reaction (reactions 3−5). In the experiments when F_2 is photolyzed, the three body

TABLE 5: Mechanism for the Methyl Formate Peroxy Reactions

	reaction[a]	rate constant[b]	ref
	Initial Reactions		
1a	$RH + Cl \rightarrow R^{\bullet} + HCl$	1.4×10^{-12}	8, 19, 20
1b	$RH + F \rightarrow R^{\bullet} + HF$	5×10^{-11}	est[c]
2	$R^{\bullet} + O_2 \rightarrow RO_2^*$	5×10^{-12}	est[c]
3	$R^{\bullet} + X_2 \rightarrow RX + X$	$(2.5-8) \times 10^{-12}$	est[c]
4	$R^{\bullet} + X \rightarrow RX$	2×10^{-10}	est[c]
5	$R^{\bullet} + R^{\bullet} \rightarrow RR$	5×10^{-11}	est[c]
6	$F + O_2 + M \rightarrow FO_2 + M$	$4.4 \times 10^{-33} P_{tot}$	18, 25
	Peroxy Reactions		
7	$RO_2^* \rightarrow CH_2OC(O)OOH$	see text	this work
8	$CH_2OC(O)OOH \rightarrow CH_2O + OH + CO_2$	see text	this work
9	$RO_2^* + M \rightarrow RO_2 + M$	see text	this work
10	$RH + OH \rightarrow R^{\bullet} + H_2O$	1.7×10^{-13}	6
11	$RO_2 + RO_2 \rightarrow 2RO + O_2$	$(2.3 \pm 0.7) \times 10^{-11}$	this work
12	$RO_2 + Cl \rightarrow RO + ClO$	2.5×10^{-10}	this work
13	$CH_3OC(O)O \rightarrow CH_3O + CO_2$	$\sim 1 \times 10^6\ s^{-1}$	est[c]
14	$CH_3O + O_2 \rightarrow CH_2O + HO_2$	2.0×10^{-15}	18
	Secondary Reactions		
15a	$CH_3OC(O)O_2 + HO_2 \rightarrow CH_3OC(O)OOH + O_2$	2×10^{-11}	est[c]
15b	$CH_3OC(O)O_2 + HO_2 \rightarrow CH_3OC(O)OH + O_3$	2×10^{-11}	est[c]
16	$CH_2O + Cl \rightarrow HCO + HCl$	7.3×10^{-11}	18, 25
17	$HCO + O_2 \rightarrow HO_2 + CO$	5.5×10^{-12}	18, 25
18	$HO_2 + HO_2 \rightarrow HOOH + O_2$	2.1×10^{-12}	18, 25

[a] R represents either CH_3OCO or $CH_2OC(O)H$ for conditions where there is no distinction between the isomers. X represents either Cl or F atoms. [b] Units are (cm^3 $molecule^{-1}$ s^{-1}) unless otherwise noted. All rate constants are reported for 298 K. [c] Rate constants are based on estimates from analogous reactions as listed in the NIST chemical kinetics database (ref 18).

addition of F to O_2 can reduce the peroxy radical yield by another 2−3% (reaction 6). The methyl formate peroxy radical, which is born with internal excitation, can then undergo either internal rearrangement followed by dissociation into formaldehyde, OH and CO_2, or it can be collisionally stabilized by the buffer gas (reactions 7−9). Any OH that is formed reacts quickly with methyl formate, extracting a hydrogen atom, thereby producing additional methyl formate radicals (reaction 10).

Once stabilized, the majority of methyl formate peroxy radicals undergo self-reaction (under our experimental conditions), producing the methyl formate alkoxy radical (reaction 11). Because the methyl formate reaction with chlorine atoms is slow compared to other hydrocarbons, such as ethane or dimethyl ether, a sufficient concentration of chlorine atoms remains long enough to react with methyl formate peroxy radicals and produce ClO. This can lead to as much as a 30% loss of RO_2 (reaction 12).

The $CH_3OC(O)O$ alkoxy radical produced from degradation of the $CH_3OC(O)O_2$ peroxy is expected to dissociate rapidly into methoxy radical and CO_2. The fate of methoxy radical is reaction with oxygen to produce HO_2 and formaldehyde (reactions 13 and 14). It is expected that HO_2, formaldehyde, as well as other degradation products will undergo further reactions (reactions 15−18), but these reactions do not substantially perturb the methyl formate peroxy self-reaction chemistry. The overall methyl formate peroxy concentrations at their maximums were found to be approximately 60−80% of the initial Cl radical concentration and 80−90% of the initial F radical concentration. The following experimental results will be discussed in terms of this reaction mechanism.

1. Methyl Formate Peroxy + Cl Reaction. Due to the relatively slow rate of reaction between Cl and methyl formate ($k_{1a} = 1.4 \times 10^{-12}$ cm^3 molecule^{-1} s^{-1})[8,19,20] the number of chlorine atoms that survive sufficiently long to react with methyl formate peroxy is much greater than for most alkyl hydrocarbons. A possible approach to reduce the peroxy plus Cl reaction is to increase the methyl formate concentration and, thereby, speed up the chlorine atom loss rate. This was not feasible in the present experiments due to the difficulty in obtaining a stable flow of gaseous methyl formate at partial pressures above 6 Torr and because high concentrations of methyl formate make the 200−240 nm region optically black. Substituting fluorine for chlorine in the mixture eliminates peroxy loss by this path because the F atoms are removed at a faster rate by reaction with methyl formate than chlorine atoms. However, using chlorine photolysis allowed measurements to be taken at pressures as low as 10 Torr, which could not be done with fluorine, owing to the F_2 precursor concentrations needed. The presence of ClO in appreciable concentration affects the calculations of both the methyl formate peroxy UV spectrum and its self-reaction rate. ClO absorbs between 210 and 310 nm, which overlaps the region of interest for the methyl formate peroxy radical. This made it necessary to determine the ClO concentration from the measured UV spectra so that corrections could be made to the absorbance spectrum as well as to the RO_2 concentration.

Figures 3 and 4 illustrate high-resolution UV spectra taken at various total pressures and gas mixtures that show the distinct features of ClO between 275 and 300 nm. These spectra were used to determine its concentration and to estimate the rate constant for the RO_2 + Cl reaction. It was found that both the ratio of initial Cl atoms to methyl formate and the total pressure were the strongest variables dictating ClO production. Higher Cl_0/methyl formate ratios result in larger ClO yields because a greater number of Cl atoms survive to react with the peroxy radicals (Figure 3). As the total pressure is increased, more of the methyl formate peroxy is collisionally stabilized and is available to react with Cl atoms (Figure 4). The RO_2 + Cl rate constant ($k_{12} = (2.5 \pm 1.1) \times 10^{-10}$ cm^3 molecules^{-1} s^{-1}) at 298 K was determined by fitting the observed ClO production to the kinetics model based on the reactions listed in Table 5.

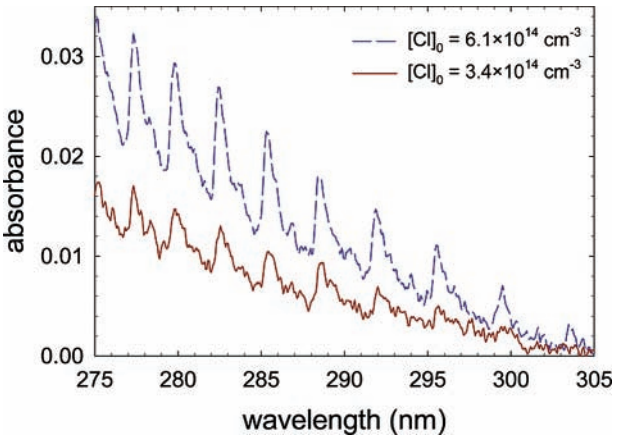

Figure 3. UV measurements of ClO radical under high and low initial Cl atom concentrations at 298 K. The methyl formate pressure is 5.5 Torr, the O_2 pressure is 12 Torr, and total pressure is 220 Torr in both cases.

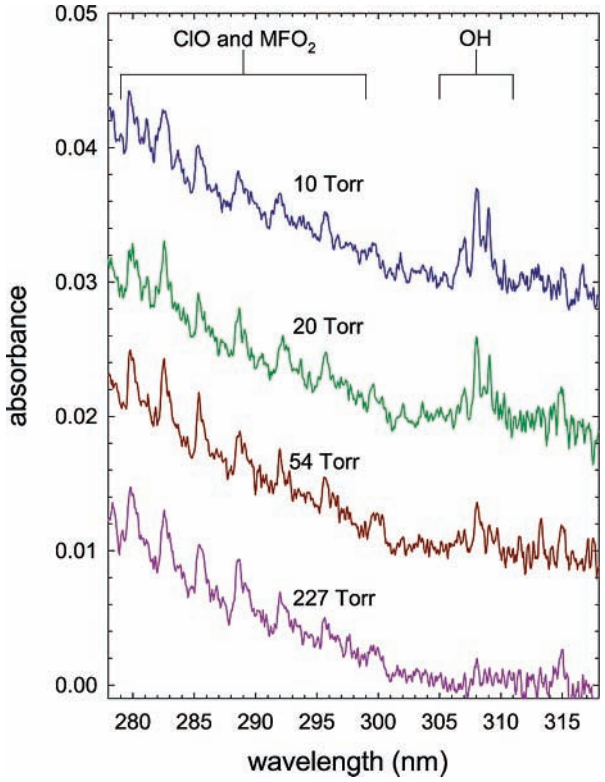

Figure 4. UV spectra of the OH and ClO radicals production as a function of pressure at 298 K. The methyl formate pressure is 5−6 Torr, whereas the O_2 pressure is 5 Torr when $P_{tot} = 10$ Torr, and 12 Torr at the higher total pressures. For visualization purposes the spectra have been separated by baseline offsets in increments of 0.01.

The main source of error in calculating the rate constant for this reaction was in determining the concentration of ClO from the UV absorbance spectra (±16%). Additional sources of error in this rate constant, which were common to all of the experiments, are described later in the results section.

2. Dissociation vs Collisional Deactivation of the Nascent Peroxy Radical. The results from the computational investigation

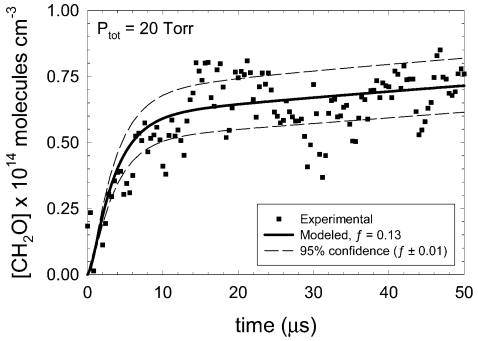

Figure 5. IR measurement of CH_2O concentration as a function of time to show the fraction of methyl formate peroxy that dissociates. The ethyl formate pressure is 5.10 Torr, the O_2 pressure is 13 Torr, and the initial Cl atom concentration is 4.98×10^{14}/cm^3. The solid line is the CH_2O concentration calculated from the kinetics model using the predicted branching ratio ×a6 = 0.13 ± 0.01. Dotted lines indicate the 95% confidence limits.

of the methyl formate peroxy radical ground state potential energy surface show that some fraction of the vibrationally excited methyl formate peroxy radicals can undergo unimolecular dissociation. The fraction that dissociates (reactions 7 and 8) is indicated by the formation of both OH radicals and CH_2O at delay times <20 μs after the photolysis laser pulse. The rate limiting step in this process is the methyl formate + Cl (or F) reaction (reaction 1). High-resolution UV spectroscopy over the range 275−320 nm provides a measure for OH production. Figure 4 shows the OH absorption spectra as a function of total pressure in the reaction cell. It is seen that as the pressure increases, the amount of OH radical produced at early times (i.e., 10 μs) decreases. The maximum observed OH yield is ∼15% at 10 Torr, which is expected to slightly underestimate the total amount of OH produced due to loss of OH by reaction with methyl formate.

Transient IR detection of the CH_2O fragment provides another measure of the branching ratio for collisional stabilization versus unimolecular dissociation of the methyl formate peroxy radical. Figure 5 shows a typical time versus concentration profile for the production of CH_2O at 20 Torr. The trace exhibits two distinct phases: The rapid initial rise in CH_2O concentration is due to the unimolecular dissociation of nascent methyl formate peroxy radicals, and the slower secondary rise comes from the oxidation of CH_3O radicals formed by the methyl formate peroxy self-reaction (reactions 13 and 14). In Figure 5, the solid line through the experimental data points represents the predicted CH_2O using the kinetics model in Table 5, and the dashed lines indicate the 95% confidence interval. The branching ratio was determined as a function of pressure over the range of 10−220 Torr (Figure 6) with the most significant changes in this ratio occurring between 10 and 75 Torr.

The resulting branching ratio can be described via a modified Lindemann mechanism. The mechanism as it was used in this work can be described by the following reactions:

$$R^{\bullet} + O_2 \rightarrow RO_2^* \qquad \text{(R2)}$$

$$RO_2^* \rightarrow CH_2OC(O)OOH \qquad \text{(R7)}$$

$$CH_2OC(O)OOH \rightarrow CH_2O + OH + CO_2 \qquad \text{(R8)}$$

$$RO_2^* + M \rightarrow RO_2 + M \qquad \text{(R9)}$$

The overall rate constant for oxygen addition to methyl formate radical

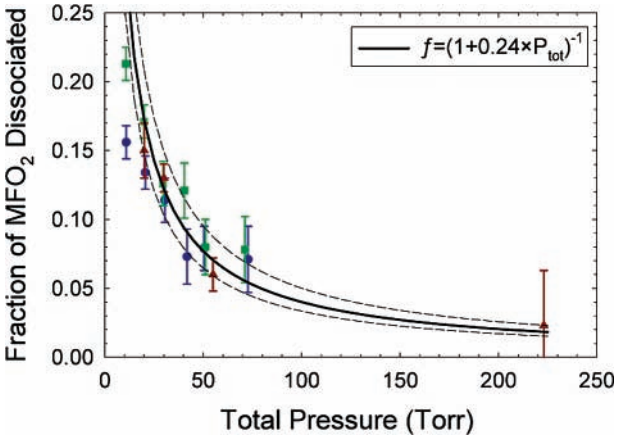

Figure 6. Pressure dependence of the methyl formate peroxy dissociation. The symbols (●, ■, ▲) indicate different initial conditions of methyl formate and Cl atom concentrations, and the solid line is the calculated fit using a modified Lindemann equation.

$$k_{total} = k_{RO_2}[M] + k_{CH_2O} \qquad (3)$$

represents the sum of the two competing processes: k_{RO_2} is the rate constant for collisional stabilization (reaction 9), where [M] is the total gas concentration, and k_{CH_2O} is the rate constant for peroxy dissociation (reaction 7). The fraction of methyl formate peroxy that dissociates is then given by

$$f = \frac{k_{CH_2O}}{k_{total}} = \left(1 + \left(\frac{k_{RO_2}[M]}{k_{CH_2O}}\right)\right)^{-1} \qquad (4)$$

If [M] is set to the total pressure, and B is defined as the ratio k_{RO_2}/k_{CH_2O} the branching fraction has the following pressure dependence:

$$f = \frac{1}{(1 + BP_{total})} \qquad (5)$$

The measured branching fractions from three different sets of conditions (Figure 6) were used to determine the parameter $B = 0.24$. The experimental branching ratio is shown to decrease rapidly from a maximum of ∼18% at 10 Torr to a low of ∼2% at 220 Torr. The measured concentration of CH_2O at the lower pressures may be underestimated due to the possibility that a fraction of the formaldehyde is born with vibrational excitation and is not probed by our IR laser until it has been collisionally relaxed. This may also be responsible for the increase in data scatter below 30 Torr. Normally a quenching gas, such as C_2F_6, can be added to quickly relax the CH_2O; in the present experiments the relatively large quantities of methyl formate used may play this role. The fit of the data to the modified Lindemann equation (eq 5) was done for pressures above 30 Torr to reduce the influence of the uncertainties at low pressure. At higher pressures, pressure broadening decreases the CH_2O detection sensitivity and causes the uncertainties in the measured concentrations to increase from 8% at 10 Torr up to 20% at 75 Torr. Other sources of error for these measurements include the IR cross section of CH_2O at the 1709 cm^{-1} line (±10%) and the initial chlorine radical concentration generated by the photolysis pulse (±5%). The overall uncertainty in the predicted fraction of methyl formate dissociation is then ±25%, or $B = (0.24 \pm 0.06)$.

3. UV Cross Section of Methyl Formate Peroxy. The UV absorbance spectrum for methyl formate peroxy was measured using the photolysis of both chlorine and fluorine to initiate

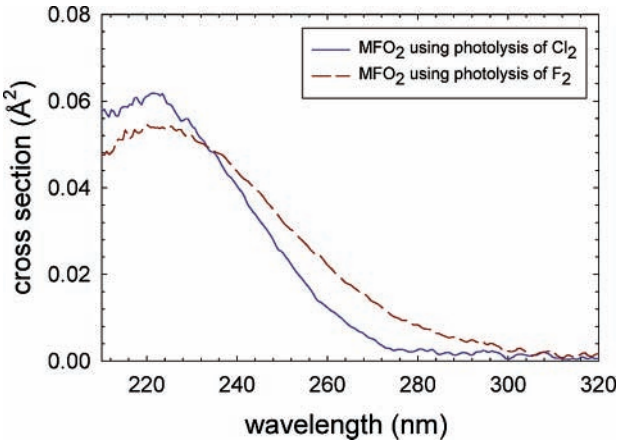

Figure 7. Composite UV cross sections of methyl formate peroxy (CH_3OCOO_2 and $O_2CH_2OC(O)H$) initiated by photolysis of Cl_2 or F_2.

the chemistry. Because it was not possible experimentally to generate either of the two methyl formate peroxy isomers separately, the measured absorbance spectra represent the combined contribution from each of the isomers weighted by the fraction of each produced. These composite absorbances were corrected for other absorbing species (methyl formate, chlorine, and ClO) before determining the methyl formate peroxy radical UV spectra. These corrections resulted in at most a 6% change at 212 nm (methyl formate) and a 25% change in the absorbance spectrum at 266 nm (ClO). When fluorine photolysis was used, the only substantial correction to the UV absorption spectra arises from accounting for the methyl formate contribution. Absorption spectra were taken under a variety of conditions of pressure, gas mixture, and initial radical concentration. The calculated cross sections from these measurements were averaged to generate the composite peroxy radical cross sections shown in Figure 7.

The two methods for producing the methyl formate peroxy radicals provide the opportunity to determine the individual UV absorbances of its two isomers, ($CH_3OC(O)O_2$ and $O_2CH_2OC(O)H$). Previous studies have concluded that in the methyl formate + chlorine reaction, the formyl hydrogen is preferentially extracted 58% of the time.[9,21] When fluorine is used, ab initio results from this study predict the branching fraction for formyl hydrogen extraction to be 19%. These differences in reactivity allow for the composite peroxy spectra to be described in terms of the two peroxy isomer absorption cross sections:

$$\sigma(\lambda)_{\text{total,Cl}} = (0.58)\sigma_{CH_3OC(O)O_2} + (0.42)\sigma_{O_2CH_2OC(O)H} \quad (6)$$

$$\sigma(\lambda)_{\text{total,F}} = (0.19)\sigma_{CH_3OC(O)O_2} + (0.81)\sigma_{O_2CH_2OC(O)H} \quad (7)$$

Simultaneous solution of eqs 6 and 7 yields the individual $CH_3OC(O)O_2$ and $O_2CH_2OC(O)H$ cross sections. Parts a and b of Figure 8 show the two deconvolved spectra along with the corresponding predictions from ab initio calculations. A Gaussian probability distribution with the appropriate standard deviation that most closely resembles the experimentally determined full width at half-maximum of the $CH_3OC(O)O_2$ and $O_2CH_2OC(O)H$ spectrum was used in conjunction with the calculated vertical transition energies to generate the calculated spectra. The resulting calculated spectrum was then multiplied by a scaling factor designed to best match the experimental cross section for visualization purposes.

The errors in the measured peroxy radical cross sections are determined as follows. The kinetics model in Table 5 is used to predict the methyl formate peroxy concentration as well as the change in methyl formate, chlorine (or fluorine), and ClO concentrations. Known rate constants are acquired from the NIST Chemical kinetics database.[18] In cases where an experimental rate constant is unknown, an estimate is made on the basis of analogous reactions. A sensitivity analysis of the model varies the following parameters: the rate constants for methyl formate radical + O_2 (k_2) and methyl formate peroxy + Cl (k_{12}) and the dissociation branching ratio (f). Errors in rate constants k_2, and k_{12} contribute ±21% to uncertainty in the cross section. Because the UV cross sections were measured at $P_{tot} > 150$ Torr, and hence $f < 3\%$, the uncertainty in f has no significant effect. Those rate constants that had to be estimated were varied by an order of magnitude to verify that the model was not sensitive to the estimated values. There are additional uncertainties of ±2% in the initial concentrations of methyl formate, O_2, and Cl_2, and ±5% in the initial chlorine atom concentrations. Noise in the measured absorbance spectra and the uncertainty in path length each contribute errors of ±2%. The branching ratio for both the Cl + methyl formate and F + methyl formate reactions were varied ±10%. The largest effect was observed in the intensity of the $CH_3OC(O)O_2$ spectrum, which was increased at its maximum, at 225 nm, by 10%. The correction for the ClO absorbance in the methyl formate peroxy spectrum that was measured under Cl_2 photolysis conditions was varied by ±15%. This affected the shape of the $CH_3OC(O)O_2$ spectrum within the strongest part of the ClO absorption region of 250−280 nm but did not affect the intensity or shape of the spectrum below 240 nm. The maximum change in the $CH_3OC(O)O_2$ spectrum intensity was ±0.005 Å^2, which is ±7% of the peak cross section. This change occurs around 270 nm, which is where the absorbance due to methyl formate peroxy is approaching zero and affects the spectrum baseline (Figure 8A). The statistical combination of these errors results in a ±27% error in the intensities of the individual methyl formate peroxy radical spectra.

4. Peroxy Self-Reaction. Figure 9 depicts a typical time versus concentration decay plot for methyl formate peroxy radicals. At the earliest times (<50 μs) the shape of the spectrum corresponds to the methyl formate peroxy spectrum. As the reaction proceeds to around 200 μs, the shape of the absorption peaks remains fairly consistent but grows weaker as the peroxy radical is removed. At times longer than 200 μs the band maximum for the absorption spectra shifts to the red, indicating a new species is being produced. Spectra obtained at delay times long enough for the complete removal of the peroxy radicals (>10 ms) show a weak absorbance with a band center around 255 nm. This residual absorbance can be accounted for by the presence of a small amount of ozone, which is expected from the cross reaction between HO_2 and $CH_3OC(O)O_2$ (reactions 15a and 15b). The $O_2CH_2OC(O)H$ radical also reacts with HO_2 but does not produce ozone. Using an estimated rate constant of 4×10^{-11} cm^3 molecule^{-1} s^{-1} for the $CH_3OC(O)O_2 + HO_2$ reaction and assuming a 50/50 branching ratio between 15a and 15b provide good agreement with the measured concentration of ozone at the longer delay times (Figure 10).

Although the individual UV spectra for the two methyl formate peroxy isomers were calculated in the previous section, their similarity to each other in shape and strength as well as the uncertainties in their deconvolution preclude their use to calculate the individual peroxy isomer concentrations. Instead, the appropriate composite methyl formate peroxy radical spectrum (for either chlorine or fluorine photolysis) is employed in the spectral fits. By using eq 1 to fit the time-resolved UV spectra of the reaction mixture to the methyl formate peroxy

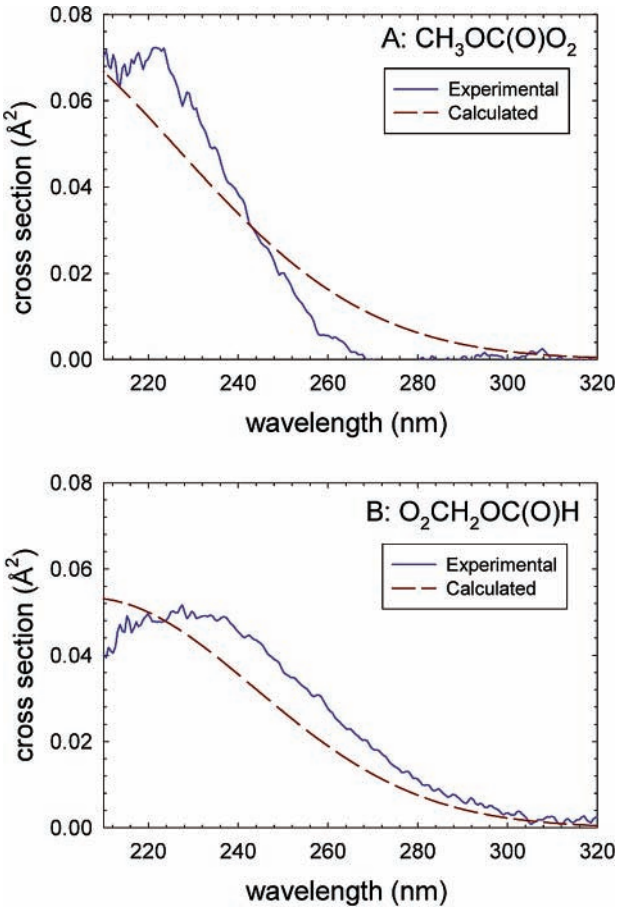

Figure 8. (a, b) Deconvolved methyl formate peroxy UV cross section for the $CH_3OC(O)O_2$ and $O_2CH_2OC(O)H$ radicals with the calculated UV spectrum superimposed on top.

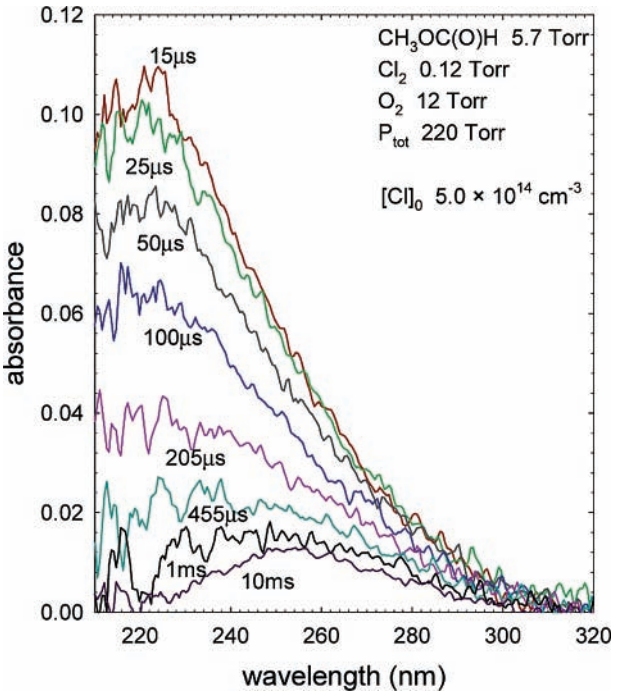

Figure 9. Typical UV time-resolved spectra of methyl formate peroxy radical self-reaction at 298 K.

radical spectrum, along with the spectra for methyl formate, O_3 and ClO, for chlorine initiation (methyl formate and O_3 for fluorine initiation), the concentrations of these species could be determined as a function of the time after photolysis. The

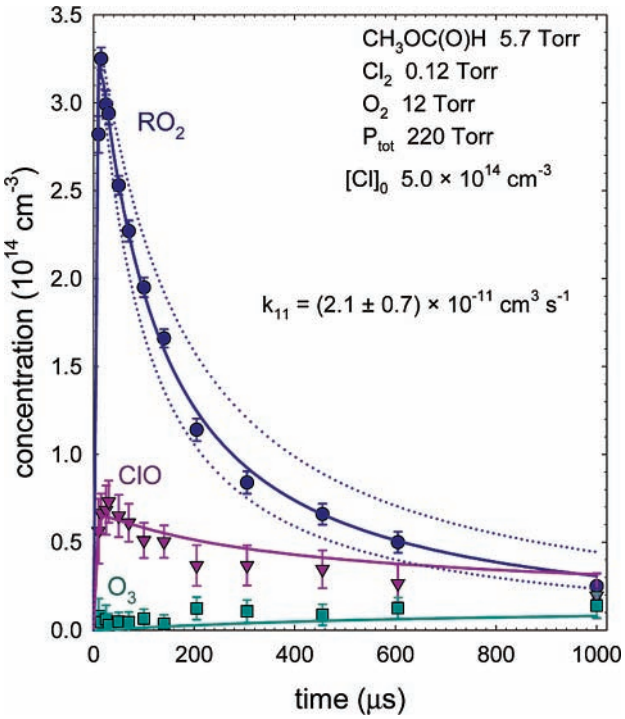

Figure 10. Concentration versus time profiles for methyl formate peroxy (●), ClO (▼), and O_3 (■) obtained by deconvolution of the time-resolved spectra from Figure 9. The solid lines show the fit of the kinetics model from Table 5 to the methyl formate peroxy radical concentrations. The dashed lines indicate $k_{11} \pm \sigma$.

profiles of species concentrations versus delay time from a measurement of the methyl formate peroxy self-reaction kinetics are shown in Figure 10. Fits of these data to the kinetics model of Table 5 yield the self-reaction rate constant of $k_{11} = (2.3 \pm 0.7) \times 10^{-11}$ cm^3 molecule^{-1} s^{-1} at 298 K, which is an average of the self-reaction rate constants for both of the peroxy isomers. In the kinetics model, the two peroxy isomers are treated separately, due to the different products from each, however, the data only permit the model to fit the total peroxy radical concentration. As a result, the model cannot predict the self-reaction rate constants of the individual peroxy isomers. Figure 10 shows that there is good agreement between the concentration of methyl formate peroxy radicals obtained from the deconvolved absorbance spectra and the calculated concentration profile. It is also shown in the figure that the kinetics model predicts the concentrations of the other measured species, ClO and O_3, very well. The dashed lines on the methyl formate peroxy fit show the effect produced by changing the self-reaction rate constant, k_{11}, by one standard deviation. However, the predicted ClO and O_3 concentrations are not affected by this change in k_{11}, because the rate-limiting reactions in the kinetics of the other products are $RO_2 + Cl$ for ClO and $CH_3OC(O)O_2 + HO_2$ for O_3. Table 6 lists the experimental kinetics trials that were carried out at pressures between 20 and 220 Torr, using the photolysis of both F_2 and Cl_2. The reported value for the rate constant is the average from trials 3−6, which were done at pressures above 150 Torr to avoid the complications caused by methyl formate peroxy radical dissociation at low pressures. The faster observed rate constant in trials 1 and 2 is a result of the inability of the kinetic model to accurately predict the fraction of methyl formate peroxy that dissociates at low pressures. As was discussed previously, the fraction of methyl formate peroxy that unimolecularly dissociates was determined by measurement of the production of CH_2O. An error analysis

TABLE 6: Measured Rate Constants for the Methyl Formate Peroxy Self-Reaction at 298 K

trial	P_{tot} (Torr)	$[Cl]_0$ (10^{14} cm^{-3})	f	k_{11} (10^{-11} cm^3 s^{-1})
1	20	4.7	0.17	5.2 ± 0.7
2	54	5.1	0.07	3.5 ± 0.5
3	166	4.7	0.02	2.5 ± 0.3
4	227	4.9	0.02	2.2 ± 0.2
trial	P_{tot} (Torr)	$[F]_0$ (10^{14} cm^{-3})	f	k_{11} (10^{-11} cm^3 s^{-1})
5	190	4.7	0.02	2.1 ± 0.7
6	226	4.0	0.02	2.2 ± 0.4

similar to the one described in the preceding section yields an overall uncertainty of ±30% in the self-reaction rate constant.

IV. Discussion

A. Rearrangement and Dissociation of the Initially Formed Methyl Formate Peroxy Radical. The methyl formate peroxy radical yield depends on a number of factors, among them the rate of hydrogen abstraction from methyl formate, the branching fraction for unimolecular dissociation of the newly formed radical, interference from the Cl + RO_2 reaction, and removal by self-reaction. Consequently, extracting kinetic data from the flash photolysis experiments requires a comparison of the data to a complex kinetic model that includes a number of reactions with unknown, or uncertain, rate constants. The strength of the present work is that the model predictions are compared simultaneously to data for a number of participating chemical species, including the methyl formate peroxy radicals, formaldehyde, hydroxyl radical, and chlorine monoxide, to help ensure consistency in the model.

Observations that the C_2H_4 and HO_2 yield from the C_2H_5 + O_2 reaction increases with decreasing pressure provided some of the first evidence that oxygen addition to alkyl radicals may proceed via an activated peroxy radical.[22] Subsequent work on dimethyl ether oxidation demonstrated that the initially formed peroxy radical can undergo an internal hydrogen atom shift from the methyl group to the peroxy moiety, and subsequently proceed via bond cleavage to produce two formaldehyde molecules and a hydroxyl radical.[23,24] Figure 1 illustrates the reaction mechanism along the dissociation channel calculated by ab initio methods. The first transition state in the unimolecular dissociation channel of methyl formate peroxy involves the rearrangement of the $CH_3OC(O)O_2$ radical to $CH_2OC(O)OOH$. The activation barrier is calculated to be 6.7 kcal mol^{-1}, less than the excess energy available from the O_2 addition. This rearrangement is followed by unimolecular dissociation to produce CH_2O, CO_2, and OH radical over a modest 7.1 kcal mol^{-1} transition state, which is again small compared to the available energy. Thus, the observation of OH and CH_2O formation is neither kinetically nor thermodynamically unexpected.

At low pressures, ~10 Torr, approximately 18% of newly formed methyl formate peroxy radicals were found to dissociate into CH_2O and OH. This fraction decreases to approximately 2% at 200 Torr owing to collisional stabilization of the nascent peroxy radicals. The concomitant decrease in OH yield at higher pressure leads to a 15−20% decrease in the methyl formate consumed. Under atmospheric conditions, it is expected that most of the peroxy radicals formed will be collisionally deactivated. However, laboratory conditions that use low-pressure flow cells to measure reaction rate constants or to probe the spectroscopy of these compounds must not ignore the effects of dissociation and the resulting secondary chemistry.

TABLE 7: Vertical Excitation Energies and Transition Momentsl

states	CASSCF energy (nm) (9e, 9mo)	CASSCF transition moment (au)
	$CH_3OC(O)O_2$ Radical	
1A′	211	0.002
2A′	180	0.1
3A′	154	0.006
2A″	198	0.852
3A″	168	0.775
	$O_2CH_2OC(O)H$ Radical	
2A′	1970	0.008
3A′	221	0.002
4A′	207	0.0995
5A′	200	0.0078
6A′	189	0.001

B. UV Spectra of the Methyl Formate Peroxy Isomers. Comparison of the shape, maximum absorption wavelength, and intensity of the methyl formate peroxy radical UV absorption spectrum to other peroxy radical spectra shows many similarities. Most peroxy radicals exhibit a strong, broad, featureless absorption band in the 200−300 nm wavelength region.[13] For the methyl formate peroxy radical, the absorption maximum lies at approximately 225 nm. Table 7 lists the calculated methyl formate peroxy vertical excitation energies and the transition moments for the first five excited states for both $CH_3OC(O)O_2$ and $O_2CH_2OC(O)H$. The deconvolved experimental spectrum (Figure 8a) of $CH_3OC(O)O_2$ has the band center at approximately 217 nm. The ground state of the $CH_3OC(O)O_2$ radical is the 1A″ state. The 1A′ → 2A″ transition of $CH_3OC(O)O_2$ has the largest transition moment with a calculated vertical excitation energy of 198 nm, 9% higher in energy than the experimental band center. The observed band center (Figure 8b) for $O_2CH_2OC(O)H$ is 230 nm, whereas calculations predict the 1A′ → 4A′ transition to occur at 207 nm. Thus, for both of the peroxy isomers the calculated vertical excitation energies done at the CASSCF level overestimate transition energies by 10%. Although the calculations can reasonably predict the band centers, experimental measurements are still required to provide the absolute strength and the shape of the UV spectrum.

C. Peroxy Radical Self-reaction. Kinetics measurements of the methyl formate peroxy radical self-reaction were performed at pressures between 20 and 220 Torr, using photolysis of both Cl_2 and F_2 (Table 6). Fitting the low-pressure kinetics data leads to a higher value of the self-reaction rate constant than is obtained from the high-pressure results. This is attributed to larger uncertainties in the reaction model at lower pressures, which arise from possible underestimation of the CH_2O formed by unimolecular dissociation of the nascent methyl formate peroxy radical. In these experiments it was not possible to distinguish between the $CH_3OC(O)O_2$ self-reaction, the $O_2CH_2OC(O)H$ self-reaction, or the peroxy cross reaction to separately determine rate constants for the 2 isomers. Therefore, the rate constant k_{11} represents the average for these peroxy radical reactions. If there were a significant difference in the self-reaction rates of these isomers, the kinetics for the chlorine photolysis conditions would be noticeably different from the fluorine photolysis conditions. However, the different ratios of initial peroxy isomers ($CH_3OC(O)O_2$ and $O_2CH_2OC(O)H$) produced when using either chlorine (58% and 42%, respectively) or fluorine (19% and 81%, respectively) yield the same value for k_{11}, within experimental error. The self-reaction rates for both peroxy isomers are expected to be close to the measured average value of 2.3×10^{-11} cm^3 molecules^{-1} s^{-1}.

TABLE 8: Comparison of $RO_2 + RO_2$ Self-Reaction Rate Constants

reaction	rate constant (298 K) (cm^3 $molecules^{-1}$ s^{-1})	ref
$(CH_3)_2CHC(O)O_2$ self-rxn	$1.44 \pm 0.11 \times 10^{-11}$	26
$(CH_3)_3CC(O)O_2$ self-rxn	$1.43 \pm 0.11 \times 10^{-11}$	26
$CF_3C(O)O_2$ self-rxn	$0.8 \pm 0.2 \times 10^{-11}$	27
$CH_3C(O)O_2$ self-rxn	$1.5 \pm 0.2 \times 10^{-11}$	28
$CH_3OC(O)O_2$ self-rxn	$2.3 \pm 0.7 \times 10^{-11}$	this work

Table 8 compares the methyl formate peroxy radical self-reaction rate constant to the self-reactions of analogous acyl peroxy radicals. The rate constant reported here is larger than for the other listed RO_2 self-reactions but not unreasonably so. Under atmospheric conditions methyl formate peroxy radicals are expected to follow the typical degradation pathways as other peroxy radicals. In urban environments (i.e., high NO_x), methyl formate peroxy radicals will mainly be removed by reaction with NO. Under low NO_x conditions, the major removal mechanism is expected to be via reaction with HO_2 radicals.

V. Conclusion

Flash photolysis coupled with time-resolved UV spectroscopy and transient IR detection is used to measure the methyl formate peroxy radical UV absorption spectrum, to probe the rearrangement and dissociation of the nascent peroxy radical, and to determine its self-reaction rate constant. The measured UV band center agrees within 10% with the transition energy predicted using high level ab initio calculations. The fraction of nascent methyl formate peroxy radicals that undergoes unimolecular dissociation to form CH_2O, OH, and CO_2 increases from approximately 2% at 200 Torr to about 18% at 10 Torr. The methyl formate peroxy self-reaction rate constant is measured to be $(2.3 \pm 0.7) \times 10^{-11}$ cm^3 $molecule^{-1}$ s^{-1}. In the course of this work we also determine a rate constant of $(2.5 \pm 1.1) \times 10^{-10}$ cm^3 $molecules^{-1}$ s^{-1} at 298 K for the reaction between chlorine atoms and methyl formate peroxy radicals, which is comparable with the earlier values for methyl and ethyl peroxy radicals.

Supporting Information Available: Tables of optimized geometries and vibrational frequencies. This material is available free of charge via the Internet at http://pubs.acs.org.

References and Notes

(1) Maricq, M. M.; Francisco, J. S. *Adv. Photochem.* **1995**, *20*, 79.
(2) Green, C. J.; Cockshutt, N. A.; King, L. *Soc. Automotive Eng. Pub. SAE-902155* **1990**.
(3) Fleisch, T. H.; McCarthy, C.; Basu, A.; Udovich, C. *Soc. Automotive Eng. Pub. SAE-950061* **1995**.
(4) Rouhi, A. M. *Chem. Eng. News* **1995**, *44*, 37.
(5) Brooks, R. *Ward's Engine and Vehicle Technol. Update*; Ward's Communications: Southfield, MI, July 15 1995; p 3.
(6) Li, Z.; Jeong, G.; Francisco, J. S.; Hansen, J.; Good, D. A. *J. Phys. Chem. A* **1999**, *103*, 10893.
(7) Good, D. A.; Francisco, J. S. *J. Phys. Chem. A* **2000**, *104*, 1171.
(8) Good, D. A.; Hansen, J.; Kamboures, M.; Santiono, R.; Francisco, J. S. *J. Phys. Chem. A* **2000**, *104*, 1505.
(9) Wallington, T. J.; Hurley, M. D.; Maurer, T.; Barnes, I.; Becker, K. H.; Tyndall, G. S.; Orlando, J. J.; Pimentel, A. S.; Bilde, M. *J. Phys. Chem. A* **2001**, *105*, 5146.
(10) Japar, S. M.; Wallington, T. J.; Richert, J. F. O.; Ball, J. C. *Int. J. Chem. Kinet.* **1990**, *22*, 1257.
(11) Maricq, M. M.; Szente, J. J. *J. Phys. Chem.* **1992**, *96*, 10862
(12) Maricq, M. M.; Wallington, T. J. *J. Phys. Chem.* **1992**, *96*, 986.
(13) Wallington, T. J.; Dagaut, P.; Kurylo, M. J. *Chem. Rev.* **1992**, *92*, 667.
(14) Frisch, M. J.; Trucks, G. W.; Schlegel, H. B.; Scuseria, G. E.; Robb, M. A.; Cheeseman, J. R.; Zakrzewski, V. G.; Montgomery, J. A., Jr.; Stratmann, R. E.; Burant, J. C.; Dapprich, S.; Millam, J. M.; Daniels, A. D.; Kudin, K. N.; Strain, M. C.; Farkas, O.; Tomasi, J.; Barone, V.; Cossi, M.; Cammi, R.; Mennucci, B.; Pomelli, C.; Adamo, C.; Clifford, S.; Ochterski, J.; Petersson, G. A.; Ayala, P. Y.; Cui, Q.; Morokuma, K.; Malick, D. K.; Rabuck, A. D.; Raghavachari, K.; Foresman, J. B.; Cioslowski, J.; Ortiz, J. V.; Stefanov, B. B.; Liu, G.; Liashenko, A.; Piskorz, P.; Komaromi, I.; Gomperts, R.; Martin, R. L.; Fox, D. J.; Keith, T.; Al-Laham, M. A.; Peng, C. Y.; Nanayakkara, A.; Gonzalez, C.; Challacombe, M.; Gill, P. M. W.; Johnson, B. G.; Chen, W.; Wong, M. W.; Andres, J. L.; Head-Gordon, M.; Replogle, E. S.; Pople, J. A. *Gaussian 98*, revision A.3; Gaussian, Inc.: Pittsburgh, PA, 1998.
(15) Werner, H. J.; Knowles, P. J. *J. Phys. Chem.* **1985**, *82*, 5053.
(16) Knowles, P. J.; Werner, H. J. *Chem. Phys. Lett.* **1985**, *115*, 259.
(17) Molpro96 is a package of ab initio programs written by H. J. Werner and P. J. Knowles, with contributions from J. Almlof, R. D. Amos, M. J. O. Deegan, S. T. Elbert, A. C. Hampel, W. Meyer, K. A. Peterson, R. M. Pitzer, E. A. Reinsch, A. Stone, and P. R. Taylor.
(18) Westley, F.; Herron, J. T.; Frizzell, D.; Hampson, R. F.; Mallard, W. G.; Mirokhin, Y.; Blakeslee, D. M. *NIST Chemical Kinetics Database*; Standard Reference Database 17-2Q98; NIST: Gaithersburg, MD, 1998.
(19) Wallington, T. J.; Hurley, M. D., Ball, J. C.; Jenkin, M. E. *Chem. Phys. Lett.* **1993**, *211*, 41.
(20) Notario, A.; Le Bras, G.; Mellouki, A. *J. Phys. Chem. A* **1998**, *102*, 3112.
(21) Hansen, J. C.; Francisco, J. S.; Szente, J. J.; Maricq, M. M. *Chem. Phys. Lett.* **2002**, *365*, 267.
(22) Kaiser, E. W. *J. Phys. Chem.* **1995**, *99*, 707.
(23) Maricq, M. M.; Szente, J. J.; Hybl, J. D. *J. Phys. Chem. A* **1997**, *101*, 5155.
(24) Sehested, J.; Mogelberg, T.; Wallington, T. J.; Kaiser, E. W.; Nielsen, O. J. *J. Phys. Chem.* **1996**, *100*, 17218.
(25) DeMore, W. B.; Sander, S. P.; Golden, D. M.; Hampson, R. F.; Kurylo, M. J.; Howard, C. J.; Ravishankara, A. R.; Kolb, C. E.; Molina, M. J. Chemical Kinetics and Photochemistry data for use in Stratospheric Modeling. Evaluation number 12. JPL Publication 97-4; JPL: Pasadena, CA, 1997.
(26) Tomas, A.; Lesclaux, R. *Chem. Phys. Lett.* **2000**, *319*, 521
(27) Maricq, M. M.; Szente, J. J.; Khitrov, G. A.; Francisco J. S. *J. Phys. Chem.* **1996**, *100*, 4514.
(28) Maricq, M. M.; Szente, J. J. *J. Phys. Chem.* **1996**, *100*, 4507.